Analyst

Accepted Manuscript

ROYAL SOCIETY OF CHEMISTRY

www.rsc.org/analyst

Analysis of affinities between specific biological ligands using Atomic Force Microscopy

Xiao Hu and Cerasela Zoica Dinu*

West Virginia University, Department of Chemical Engineering, Morgantown, WV, 26506

Abstract

In the cell, protein-ligand recognition involves association and disscociation processes controlled by the affinity of the two binding partners and chemical harvesting of adnosine triphosphate energy. Fundamental knowledge of selected recognition events is currently translated in synthetic environment for biosensors, immunoassays and diagnosis applications, or for pharmaceutical development. However, in order to advance such fields, one needs to determine the lifetime and binding efficiency of the two partners, as well as the complex' energy landscape parameters. We employed contact mode atomic force microscopy to evaluate the association and dissociation events between streptavidin protein and its anti-streptavidin antibody ligand, currently used for nucleotide array, ELISA, and flow cytometry applications, just to name a few. Using biotin as control, our analysis helped characterize and differentiate multi- or single bonds of different strengths as well as associated energy landscapes to determine protein-ligand structural arrangement at nanointerfaces and how these depend on the specificity of the ligand-recognition reaction. Our results suggest that understanding the importance of the rupture forces between a protein and its ligand could serve as the first step to protect on-off switches for biomedical research applications where specificity and selectivity are foremost sought.

Introduction

Biological world maintains structure and function through operative molecular interactions. For instance, the specific interactions and high recognition affinity between antibodies and protein antigens contribute to pathogen and their product recognition to ultimately provide immune protection[1, 2]. Accordingly, protein antigen and antibody binding affinity and energetics are becoming a prominent area in therapeutics where ligand specificity influences humoral immunity[3-6].

Fundamental knowledge of molecular interactions binding affinity and strength[7] was gained mostly by studying their *in situ* characteristics using techniques relying on optical[8] and magnetic tweezers[9], or impedance spectroscopy[10]. For instance, Sischka et al., studied the dynamic translocation of ligand-complexed DNA through solid-state nanopores using optical tweezers[11], Liebesny et al., determined the number of proteins bound non-specifically to DNA using magnetic tweezers[12], while Duan et al., showed how impedance spectroscopy could be used to study the formation of a silicon nanowire field-effect transistor capable to measure protein–ligand binding affinities and kinetics with sensitivities down to femtomolar concentrations[13]. However, the implementation of such studies is currently hindered by either optical perturbations and how these affect the performance of the tweezers[14, 15], or the complexity and time scale of sample preparation and sample storage[15], and the reduced detection capability of the instrument and how instrument's overheating influences the measurement process[15] especially for protein-ligand pairs known to be heat sensitive[16].

Atomic Force Microscopy (AFM) was recently implemented to circumvent some of these drawbacks; the technology does not require a specific or tedious pretreatment of the samples, is user and environmentally friendly, and allows for nano-resolution while depicting the exquisite surface structure of the samples being investigated[17]. As such, AFM was employed to visualize the surface architecture of *Corynebacterium glutamicum* with the analyses revealing an inner layer with about 11 nm periodicity in the structure of the individual cell[18]. The interaction parameters, such as the rupture force and dissociation constant, energy landscape parameters or energy bond and energy barrier width of the biotin and streptavidin bond were also quantified using AFM[19]; biotin and streptavidin are known to form the strongest non-covalent interaction in the biological world. Complementary, AFM analysis of the newly identified protein Gli349 and sialyllactose molecules revealed an unbinding force of around 70 pN; the Gli family is involved in the gliding of the bacteria *Mycoplasma*[20]. Similarly, Ge et al., used AFM to study the specific interaction between bivalent aptamer Bi-8S and investigated the unbinding dynamics and dissociation energy landscape of their multivalent interactions[21]; the aptamer is a class of molecular probes used for protein recognition, detection, and inhibition.

Translating and implementing the knowledge of binding affinity and strength led to the development of immune deficiency syndrome (AIDS)[22] and cancer[23] detection assays. Complementary, studying the interaction of two complementary or partly matched single strands of DNA molecules helped identify DNA mutations[24] or damages[25], while self-assembly monolayer technology relying on binding and recognition at electrode interfaces is currently used in controlling deposition of nanostructures[26] or biosensor's sensitivity[27]. However, there are still fundamental questions to be answered before further implementation of biomolecular interactions in synthetic assays is to be realized. In particular, scientific endeavor is required to investigate how single molecular scale interactions at the protein-ligand binding pocket site can be distinguished from non-specific interactions such as binding at intermediate positions. Lack of specificity is associated with weaker interactions that could lead to both low sensitivity and low detection capabilities in synthetic assays such as ELISA[28] or immunodiagnostic[29-32]. Such endeavors require understanding of the basis for protein-ligand binding as well as the energetics associated with protein-ligand individual complexes formation.

To help answer these questions, we formulated a quantitative method that allowed for the ranking selection of unbinding forces between streptavidin and its ligand, namely anti-streptavidin antibody, all under known mechanical stress. By controlling the specificity of binding and limiting non-specific interactions, we showed through multi-Gaussian fitting that fine tuning of the protein-ligand interactions can help identify the disposition of protein binding site, distinguish the protein arrangement at interfaces and its influence on the energy landscape, as well as shed light into the characteristics of the protein-ligand recognition event and the association and dissociation events. Unraveling such events allowed analysis of ligand-breaking maps, all under a known mechanical force, to be used for a variety of applications from ELISA[28] to immuno-diagnosis or -reagent analysis[22,23].

Results and discussion

Applied biochemistry relies on molecular recognition as an essential element in evaluating self-replication, self-assembly, and information processing. Analysis of biomolecular recognition events performed in synthetic environment have shown that protein-ligand interactions are the key part of the bond formation, with the bond being strongly influenced by both steric hindrance[33] and protein's arrangement at a particular interface[34].

To evaluate and help rank biomolecular recognition events based on the bond energetics, we used the streptavidin-anti-streptavidin antibody complex. Streptavidin was chosen as a model protein based on previous reports that helped characterize both its structure[35] as well as its interaction with known ligand biotin[19, 36, 37].

Experimental set-up to evaluate biomolecular recognition events between a protein and its ligands

Our experimental approach used atomic force microscopy (AFM) in contact mode, streptavidin-coated surfaces and ligand-coated AFM tips and evaluated the rupture forces between proteins and their ligands at a constant trigger force. Specifically, Figure 1 shows the multi-step functionalization of glass surfaces with streptavidin. Briefly, by immersing glass slides into Piranha solution hydroxyl radicals were generated[38] and subsequently used to immobilize 3-aminopropyltriethoxysilane (APTS) to be used as "hangers" for covalent binding of glutaraldehyde (GA; Figure 1a). Streptavidin was attached to the glutaraldehyde-functionalized surfaces using the zero length EDC/NHS chemistry[39]; complementary, anti-streptavidin antibody or biotin (used as control) ligands were immobilized onto the AFM tip by using physical binding[37] (Figure 1b).

Figure 1c and Figure 1d depict the rupture force as result of engaging and de-engaging the ligand-functionalized tip from the streptavidin- coated surface under an external force controlled by the user (Figure 1c for the anti-streptavidin antibodies and 1d for biotin control). During the engaging process, the ligand-coated AFM tip came in direct contact with the streptavidin-coated surface to form ligand-protein conjugate complexes. During the tip detaching process and when the force generated by the bending of the cantilever reached the rupture force (with a more severe bent being a result of a higher rupture force between the coated tip and the streptavidin), the interaction between the ligand-coated tip and the streptavidin-coated surface was broken and recorded.

To evaluate the rupture force between streptavidin and its ligands (i.e., biotin used as control and anti-streptavidin antibodies), two different cantilevers with spring constants of 20±6 pN/nm and 90±27 pN/nm respectively, were used. Since the effective spring constant depends on the elastic properties of both the cantilever and the substrate[40], we used thermal tuning and analysis of the deflection versus

distance curve at constant room temperature to calibrate the cantilevers before each experiment[41]. Thermal tuning analysis showed spring constants of 25±5 pN/nm and 104±14 pN/nm respectively; subsequently, the resulting rupture forces of the biotin-streptavidin (control) or anti-streptavidin antibodies-streptavidin complexes were evaluated at $1.2x10^5$ pN/s and $5.4x10^5$ pN/s force loading rates, with the loading rate being determined from the rate of cantilever retraction[42]. The rate of cantilever retraction was defined as the velocity at which the tip retracted from the streptavidin-coated surface resulting in retraction values between 4800±1000 nm/s and 5192±616 nm/s respectively for the two cantilevers being considered.

Figures 2a and 2b shows the representative force maps of 1 μm × 1 μm areas where the analysis of the rupture forces between the anti-streptavidin antibodies- or the biotin-coated tip and streptavidin-coated surfaces respectively were performed. For the contact mode AFM force analysis, the area underneath the tip was divided automatically into 10×10 matrices to result in 100 parallel test areas/per experiment, with the AFM measuring the rupture force upon contact between the ligand-coated tip and each one of these matrices and providing the average force map per individual area being analyzed. Each square was color-coded with the darker color representing a smaller rupture force while the lighter color referred to a larger value of such force.

Analysis of protein-ligand rupture events

Figures 2c and 2d show the representative histograms force distribution associated with the rupture events, each derived from 100 independent matrices allowing for force measurements. For the anti-streptavidin antibody-streptavidin experiment, the rupture force ranged from 0 to 100 pN, with a dominant regime in the 25 pN to 80 pN range and two peaks (Figure 2c). The red solid line resulted from the multi-Gaussian fitting identified an average rupture force of about 42 pN with F*1 (68.7pN) presumably indicating the most probable rupture force for a single bond formed between anti-streptavidin antibodies-coated tip and streptavidin-coated surface[43,44]. The force distribution also revealed another peak centered around 12.8 pN presumably associated with the non-specific interaction between the tip and the surface or binding of the antibodies at other than the specific streptavidin pocket site. Indeed, in control experiments performed with anti-streptavidin antibodies-coated AFM tips brought in close proximity of the glass surface functionalized with only glutaraldehyde, showed a rupture force of only 12.2±6.8 pN.

For the control experiment performed between the biotin-coated tip and the streptavidin-coated surface (Figure 2d), the rupture force ranged from 5 pN to 1340 pN, with a dominant regime in the 200 to 900 pN range and with multiple peaks distribution[45]. Multi-Gaussian fit allowed identification of the

average rupture force at around 551 pN with peaks distribution at F*1 (285 pN), F*2 (636 pN) and F*3 (973 pN) respectively presumably associated with rupture events for single, double and triple bonds[46, 47]. Forces below 100 pN were presumably due to non-specific interactions of the biotin-coated tip to the streptavidin-coated surface, non-specific interactions of the biotin-coated tip at other than the structural site of the attached streptavidin or the structural arrangement of the streptavidin at the glass interface that lead to a structural packing with limited biotin binding ability[48], or an equilibrium between the association and dissociation process[49, 50] respectively. Indeed, control experiments showed that biotin-coated tips brought in close proximity of the glutaraldehyde-coated glass surfaces resulted in a rupture force of only about 8.6±7.1 pN.

Figure 3 plots the mean rupture force against the loading rate for the unbinding process of the two different ligands[51], with Figure 3a showing the loading rate dependence of the rupture force in the unbinding process of the anti-streptavidin antibody-coated tip and the streptavidin-coated surface and Figure 3b of the biotin-coated tip and the streptavidin-coated surface respectively. The analyses are based on at least 12 independent replicates performed for each of the protein-ligand complex being investigated. The red solid lines represent the linear fitting for the two protein-ligand complexes being considered, with each complex containing two regimes. Namely, for the anti-streptavidin antibody-streptavidin complex, the average rupture force between the coated tip and the streptavidin-coated surface showed a rapid decrease in the loading rate ranging from 690000 pN/s to 18400 pN/s, followed by a more gradual decrease in the 161000 pN/s to 11500 pN/s range respectively. For the control with the biotin-coated tip, the rupture force between the functionalized tip and the streptavidin-coated substrate decreased with the loading rate. The average rupture force dropped from 601 pN to 142 pN as the loading rate dropped from 150000 pN/s to 7500 pNs. However, in the slower loading rate (ranging from 2500 pN/s to 250 pN/s), the average rupture force was minimally changed (from 130 pN/s to 115 pN/s) which could be due to the association and dissociation processes between the two ligands being at equilibrium[49, 50]. Analysis also showed the presence of additional points in the loading range from 2980 to 8103 pN/s ($\ln(L_r)$=8~9) which were identified as being contained in a so-called “intermediate region”.

Kinetics of the association and dissociation of protein-ligand complexes recognition events

For the quantitative analysis of the unbinding characteristics of the protein-ligand complexes, we employed Bell-Evans model[52, 53] and Kramer's theory[54] and evaluated the dissociation rates and energy barriers. Briefly, Bell-Evans model predicts a linear relationship between the rupture force and the logarithm of the loading rates[44], with the dissociation of the protein-ligand complex under an external force being correlated to the applied external force[55] by:

$$k(F) = k_0 \exp(\frac{Fx^{\neq}}{k_B T}) \quad (1),$$

where k(F) is the off-rate of protein-ligand dissociation that depends on the external force being applied ($F_x^{\neq}$), k_0 is the dissociation rate constant in the absence of an external force, k_B is the Boltzmann constant, T is the absolute temperature, and $x^{\neq}$ is the energy barrier width which relates to the distance between the binding partners and the transition state projected along the direction of the applied force[53]. As the applied force increased with time and the deformation of the cantilever, the likelihood of any bond formed between the tip and the surface to be broken also increased, allowing for the probability density (P) of the "surviving" population of bonds to be calculated function of the failure of a single bond and the time required to break that bond, i.e., t, respectively using:

$$P(t,F) = k(F) \exp(-\int_0^t k(f(t'))dt) \quad (2),$$

P has a maximum value when dP/dF=0 and $F=F_{max}$ respectively, where F_{max} refers to the maximum force that could lead to the protein-ligand dissociation in one binding event and is function of the rupture force and loading rate through:

$$k(F_{max}) = L_r \frac{\partial}{\partial F} \ln(F) \mid_{F=F_{max}} \quad (3).$$

By combining equations 1 and 3, and considering a constant loading rate L_r, the resulting unbinding force is:

$$F = \frac{k_B T}{x^{\neq}} \ln(\frac{L_r x^{\neq}}{k_0 k_B T}) \quad \text{or} \quad F = \frac{k_B T}{x^{\neq}} \ln(\frac{x^{\neq}}{k_0 k_B T}) + \frac{k_B T}{x^{\neq}} \ln(L_r) \quad (4).$$

From equation (4), the dissociation rate constant (k_0) for anti-streptavidin streptavidin and streptavidin-biotin (control) respectively were calculated and included in Table 1. Specifically, based on the linear fitting of the average rupture force versus the natural logarithm of the loading rates for anti-streptavidin antibodies-streptavidin in Figure 3a, the linear equations for the higher loading and lower loading rate regions respectively were: F= 41.98 ×

$\ln(L_r) - 490.4$, and $F = 2.301 \times \ln(L_r) - 7.513$. The resulting dissociation rate constants, k_0 of the anti-streptavidin antibody-streptavidin complex were thus 2814 s^{-1} and 10.19 s^{-1}, while the energy barrier widths, $x^{\neq}$, were 0.097 nm and 1.73 nm.

Analyses also showed that the values of the dissociation rate constants were smaller for the anti-streptavidin-streptavidin complex when compared to control biotin-streptavidin complexes thus suggesting that the bond lifetime ($1/k_0$) of the anti-streptavidin-streptavidin complex is much smaller than that of the control. Specifically, the linear equations for the higher loading rate region (i.e., $F = 4.862 \times \ln(L_r) + 86.78$), allowed determination of k_0 as 24.94 s^{-1} and energy barrier width ($x^{\neq}$) as 0.031 nm for the control. Complementary, for the lower loading rate region, the linear equation was $F = 133.87 \times \ln(L_r) - 1084.01$ while the dissociation rate constant k_0 was 3.64×10^{-9} s^{-1} and $x^{\neq}$ was 0.84 nm.

The above analyses confirmed previous studies that showed that there were at least two energy barriers (defined as inner and outer barriers respectively) for the biotin-streptavidin complex used as control, both presumably associated with the biotin binding close to the streptavidin pocket conformation (inner barrier) or at the last state before the unbound conformation (outer barrier)[37, 46]. Similar results were obtained by Yuan et al., (0.05 nm)[43] and Piramowicz et al., (0.024±0.003 nm)[56] for the inner barrier, while for the outer barrier the results were 0.49 and 0.53 nm (Yuan et al.,[43]) and 0.38±0.21 nm (Rico et al.,[37]) respectively. The observed values were presumably related to the H-bond ruptures events as determined by the structural packing of the individual protein-ligand and the symmetry of the streptavidin tetramer itself[46], with the outer energy barrier being attributed to the steric hindrance generated by the Trp120 amino acid which prevents the biotin from escaping during the unbinding process[46]. Yuan et al.,[43] also found that the outer barrier width decreases (from 0.49 nm to 0.31 nm) while the k_0 dissociation constant increases (from 1.67×10^{-5} s^{-1} to 6.70×10^{-3} s^{-1}) after they used a truncated form of streptavidin with the Trp120 changed to Phe120.

Activation energy determination is function of the individual protein-ligand interactions

Using Kramer's theory that describes the kinetic off rate for unbinding of the two partners in the individual complex and equation 4, we calculated the activation energy of the protein-ligand interaction from the intercept and the slope in the individual linear fittings respectively, where the individual fittings were based on analysis of 12 independent replicates as:

$$L_{r,F=0} = \omega f_B \exp\left(\frac{-\Delta E}{k_B T}\right) \quad (5)$$

where ω is the frequency prefactor, f_B is $k_B T / x^{\neq}$ with ΔE being the activation energy[51].

$$\frac{\Delta E}{k_B T} = -\ln(L_{r,F=0}) + \ln(f_B\,\omega) \approx -\ln(L_{r,F=0}) + \ln(f_B) \quad (6)$$

By substituting k_B and $x^{\neq}$ into equation (6), the activation energies of the biotin-streptavidin complex was calculated as -3.20 k_BT for the higher loading rate region and 19.44 k_BT for the lower loading rate region respectively. Previous research showed that the activation energy for the biotin-streptavidin was in the range of 2.90 k_BT to 35.91 k_BT[57, 58].

The difference in between our and previously reported results is presumably related to the complexity of the experimental set-up in which both the loading rate range (that controlled the rupture events) and the surface functionalization method (that controlled attachment and packing of the ligand or the protein at their respective interfaces) were different. In particular, considering that each streptavidin when free in solution has 4 binding pockets for biotin, with the number of pockets decreasing upon protein immobilization, and considering that the very end of the tip is a square with the radius of 42 nm where the size of the biotin is about 3 nm, the set-up geometry will allow for a large number of binding events to occur. Such events could lead to multi-bonds formation, all function of the overall distance of the coated cantilever from the substrate, the loading rate regime applied, the distribution of the binding pockets, the geometry of the protein and its ligands, as well as hindrance effects. These were confirmed by analyzing the "intermediate region" in which the outer barrier is governed by different interactions than the ones that govern the inner barrier also suggesting high enantioselectivities[59] of the two binding partners, with the negative energies being presumably associated with conformational changes due to the binding of the ligand at other than the streptavidin pocket binding site itself[60].

For the anti-streptavidin antibody-streptavidin complex, the activation energies were -7.94 k_BT for the higher and -2.32 k_BT for the lower loading rate regions respectively. Similar results were obtained for other antibody-antigen pairs with research showing an activation energy of - 6.37 k_BT for the arginine-glycine-aspartate (RGD) and human platelet $\alpha_{IIb}\beta_3$ pair[61] or - 6.4 k_BT for the RGD and fibrinogen pair[62]. The negative values may illustrate that the binding event is not a two-state-one-step type, but it contains an intermediate step[63] most likely associated with the re-arrangement of the two binding partners at the interfaces they were immobilized onto. The different values of the activation energy may also be due to the model being considered for the analysis[64]. It is arbitrarily however to speculate that there were two energy barriers in the anti-streptavidin antibody-streptavidin complex since the protein-ligand interaction that leads to this complex formation is more intricate than the one for the control biotin-streptavidin. In particular, the "Y"-shaped structure of the anti-streptavidin antibody with the two light and two heavy chains[65] and its length of about 10 nm can assume at least 4 different orientations when coated onto the tip surface, i.e., "end-on fab-up", "end-on fab-down", "side-on" and "flat-on"[65].

Such orientations could presumably lead to reduced number of binding events with the protein-coated surface when in close proximity. While anti-streptavidin antibodies in the "end-on fab-up" structure have the highest probability to form a perfect bond with the immobilized streptavidin, other orientations resulting from either the protein or antibody's packing at their respective two interfaces, as well as steric hindrance, are likely to generate non-specific interactions and thus explain the lower energy barrier of the complex.

Controlling the specificity of protein-ligand recognition events allows for extended *in vitro* applications

The average rupture forces as resulted from all the parallel experiments performed for both anti-streptavidin antibody-streptavidin and biotin-streptavidin complexes are presented in Figure 4. As shown, the control biotin-streptavidin complex had an average rupture force of 551 ± 132 pN while for the streptavidin-anti-streptavidin antibody complex the rupture force was 50.2 ± 12 pN. The rupture forces for other sets of controls, i.e., biotin or anti-streptavidin antibodies coated to the tip and brought in close proximity to only the glutaraldehyde-coated glass surfaces, were 8.6 ± 7.1 pN and 12.2 ± 6.8 pN respectively. Those additional controls were accounted to eliminate concerns related to ligand unbinding from the tip.

The performed Student's T-test showed that the average rupture forces between biotin-streptavidin and anti-streptavidin antibody-streptavidin complexes were significant from each other and significant from their controls respectively. The differences in the average rupture forces between the two pairs of ligands confirmed previous results that allowed calculations of the activation energy. In particular, with the activation energy of the biotin-streptavidin bond being much larger than that of the anti-streptavidin-streptavidin bond, a larger force will be required to cross that energy barrier. This analysis suggests that controlling the specificity of binding and limiting non-specific interactions through fine tuning of the protein-ligand interactions can help identify the disposition of protein binding pocket site, its packing at nanointerfaces, as well as shed light into its energetic characteristics as linked to a particular sequence/structure and the protein-ligand recognition event.

Our study has the potential to advance biomedical applications. For instance, knowing that ELISA assay relies on the antibody immobilized on the substrate to capture the target that subsequently allows for a color change[28], assays can be developed to recover the antibody-antigen and make the substrate reusable. Further, by applying a known rupture force to break a specific protein-ligand bond when using controlled microfluidic flow or differentiating between "perfect" versus "imperfect" bonds, immuno-separation assays can be optimized. Specifically, by considering the orientation of the antibodies

at nanointerfaces, a higher sensitivity and selectivity could be achieved if all the antibodies will be in an "end-on fab-up" orientation to allow efficient capturing of the corresponding protein with the binding-breaking event performing as an "on-off switch" *in vitro*. Lastly, when the target binds to its receptor, the protein-ligand complex could be considered an "on" switcher while applying a specific force to break this bond will create an "off" switcher to be possibly used for diverse applications from biosensors to gene expression[66].

Conclusions

In this study, the energetics of anti-streptavidin antibody-streptavidin complex was studied by AFM and compared to that of the well-known biotin-streptavidin bond. Multi-Gaussian fitting showed that a multi-binding events occurred between the biotin-coated AFM tip and the streptavidin-coated glass surface, which are in contrast with a single binding event observed to occur between the anti-streptavidin antibody and the streptavidin surface. Results also showed that the "Y" shaped structure of the anti-streptavidin antibodies and their packing at the interfaces are more likely to form imperfect bonds with their protein ligand, thus decreasing their required rupture forces. Kinetic parameters, such as the energy barrier width, activation energy, dissociation constant of both protein-ligand complexes were obtained from Bell-Evan's model to help evaluate and categorize protein-ligand binding affinities possibly to be extended for biomedical applications.

Experimental

Functionalization of the Atomic Force Microscope (AFM) tips

TR-400PB tips (purchased from Asylum Research, USA) were functionalized with either biotin or anti-streptavidin antibodies. Briefly, the tips were first cleaned using a three steps cleaning protocol which consisted of first immersing them into 1 mL of deionized water for 10 min, secondly into acetone (Fisher Scientific, USA) for another 10 min, and lastly, in deionized water for 10 more minutes. Subsequently, the tips were dried under air, exposed to ultraviolet (UV) light for 30 min, rinsed again with 100 mM pH 7.0 phosphate buffered saline (PBS, made from mono-potassium phosphate, dipotassium hydrogen phosphate and sodium chloride, all reagents purchased from Fisher Scientific, USA) and incubated in solution of either 1 mg/mL biotin (Sigma, USA) or anti-streptavidin antibodies (Sigma, USA) for 3 h at room temperature. After incubation, the tips were rinsed in PBS to remove loosely bound ligands and used immediately.

Cleaning of glass substrates

Glass slides (d=25 mm, Corning, USA) were ultrasonicated in deionized water, 99% alcohol (Fisher Scientific, USA) and again in deionized water for 30 min each. Subsequently the slides were dried under vacuum for 1 day and before use exposed to UV light for 30 min.

Protein functionalization of the glass substrates

Streptavidin was covalently attached to the cleaned glass slides using established methods[38]. Briefly, glass slide was immersed into a Piranha solution (96.4% sulfuric acid, H_2SO_4, Fisher Scientific, USA) and 30% hydrogen peroxide (H_2O_2, Fisher Scientific, USA) in a 3:1 volume ratio, and heated to 120 ^oC for 10 min. After exposure to Piranha, the slide was thoroughly washed with deionized water and dried under vacuum for 1 day. Upon drying, the slide was immersed in 1 ml of 5% 3-aminopropyltriethoxysilane (APTS; Fisher Scientific, USA), 99.5% toluene solution (Fisher Scientific, USA) and incubated at room temperature for 1 h. Upon time elapse, the slide was again washed thoroughly with deionized water, toluene and deionized water and subsequently immersed into 1 mL 5% glutaraldehyde (Acros Organics, USA) in 0.2 M pH 9.0 Tris-buffered saline (TBS, made from tris and hydrochloric acid, reagents purchased from Fisher Scientific, USA) at room temperature, for 1 h with shaking at 200 rpm. Lastly, the slides were extensively rinsed with TBS, activated for 15 min in a 1ml solution of pH 4.7 of 2-(N-morpholino)ethanesulfonic acid (MES, Fisher Scientific, USA) containing 160 mM 1-Ethyl-3-(3-dimethylaminopropyl)carbodiimide (EDC, Acros Organics, USA) and 80 mM N-Hydroxysuccinimide (NHS, Pierce, USA) and incubated in 2 mL of 4 μg/mL streptavidin solution in

PBS at room temperature and 200 rpm for 3 h. The slides were removed from the streptavidin solution and the remaining solution was collected. Upon incubation, the streptavidin-functionalized glass slide was rinsed thoroughly with PBS to remove loosely bound proteins and the first 200 µL of the washout was also collected, added to the supernatant, and used for protein loading analysis.

Evaluation of the protein loading onto the functionalized glass slide

The amount of the streptavidin bound to the glass slides was evaluated using micro BCA protein assay (Pierce, USA) and subtracting the amount of the protein washed out in the supernatant and collected washes from the amount of the protein initially added in the incubation step. Briefly, 500 µL of working reagent containing 50 parts of reagent A, 48 parts reagent B and 2 parts of reagent C (all reagents were provided with the kit) were mixed with 500 µL streptavidin solution (either from the supernatant and or the 200 µL of the washes) and incubated at 60 ^{0}C for 1 h. After incubation and sample cooling to room temperature, absorbance at 562 nm was recorded using a UV-Vis Spectrophotometer (Thermo Scientific EVO300). Known concentrations of streptavidin in the working reagent were used to form a calibration curve.

AFM force measurement

A contact mode AFM force measurement was used to evaluate the rupture forces between biotin- or anti-streptavidin antibodies-coated tip and streptavidin-coated substrate. The trigger force was fixed to 3 nN and the spring constant of the cantilever was measured and calibrated before each experiment using established calibration method[41]. The area for each analysis was kept constant to 1 µm x 1 µm.

Statistical data analysis

In order to compare the average rupture forces, a Student T-test was carried out with the significance level of $p^{*}<0.05$; 40 parallel force map experiments per individual sample analysis (i.e., where sample is defined as either of the ligand) were performed, with at least 6 samples being analyzed at independent times. For the loading rate dependence of the rupture force there were at least 12 samples being analyzed. For each, there were at least 5 areas of 1 µm x 1 µm being considered; in each one of these areas the loading force was varied. For the biotin-streptavidin, the loading rate varied from 250 to 150000 pN/s, while for anti-streptavidin antibodies-streptavidin the loading rate varied from 11500 to 161000 pN/s. These loading rates accommodated the different spring constant as measured for individual experiments.

Acknowledgements

This work was supported by National Science Foundation (NSF) grant 1300757. The authors acknowledge the use of WVU Shared Research Facilities as well as the help of Chenbo Dong, Ph.D. for student training.

References

1. T. H. Mogensen, *Clinical Microbiology Reviews*, 2009, **22**, 240-273.
2. S. Akira, S. Uematsu and O. Takeuchi, *Cell*, 2006, **124**, 783-801.
3. A. Jamali, M. Mahdavi, Z. M. Hassan, F. Sabahi, M. J. Farsani, T. Bamdad, H. Soleimanjahi, M. Motazakker and S. Shahabi, *International immunology*, 2009, **21**, 217-225.
4. N. Abboud, S. K. Chow, C. Saylor, A. Janda, J. V. Ravetch, M. D. Scharff and A. Casadevall, *The Journal of experimental medicine*, 2010, **207**, 2395-2405.
5. S. Pouyanfard, T. Bamdad, M. Parsania, H. Hashemi and M. G. Mohammadi, *Cytokine*, 2010, **50**, 99-103.
6. H.-P. Peng, K. H. Lee, J.-W. Jian and A.-S. Yang, *Proceedings of the National Academy of Sciences*, 2014, **111**, E2656-E2665.
7. M. M. Santos, I. Marques, S. Carvalho, C. Moiteiro and V. Felix, *Organic & biomolecular chemistry*, 2015.
8. W. Zhang, W. Deng, L. Zhou, Y. Xu, W. Yang, X. Liang, Y. Wang, J. D. Kulman, X. F. Zhang and R. Li, *Blood*, 2015, **125**, 562-569.
9. D. Kilinc, A. Blasiak, James J. O'Mahony, Daniel M. Suter and Gil U. Lee, *Biophysical journal*, 2012, **103**, 1120-1129.
10. E. Zor, H. Bingol, A. Ramanaviciene, A. Ramanavicius and M. Ersoz, *The Analyst*, 2015, **140**, 313-321.
11. A. Sischka, A. Spiering, M. Khaksar, M. Laxa, J. König, K.-J. Dietz and D. Anselmetti, *J Phys Condens Matter*, 2010, **22**, 454121.
12. P. Liebesny, S. Goyal, D. Dunlap, F. Family and L. Finzi, *Journal of Physics: Condensed Matter*, 2010, **22**, 414104-414108.
13. X. Duan, Y. Li, N. K. Rajan, D. A. Routenberg, Y. Modis and M. A. Reed, *Nat Nano*, 2012, **7**, 401-407.
14. C. Wang, S. Chowdhury, S. K. Gupta and W. Losert, *Journal of biomedical optics*, 2013, **18**, 045001.
15. K. C. Neuman and A. Nagy, *Nat Meth*, 2008, **5**, 491-505.
16. T. Ulrichs, A. M. Drotleff and W. Ternes, *Food chemistry*, 2015, **172**, 909-920.
17. D. J. Müller and Y. F. Dufrêne, *Trends in Cell Biology*, 2011, **21**, 461-469.
18. S. Scheuring and Y. F. Dufrêne, *Molecular Microbiology*, 2010, **75**, 1327-1336.
19. S. Guo, C. Ray, A. Kirkpatrick, N. Lad and B. B. Akhremitchev, *Biophysical journal*, 2008, **95**, 3964-3976.
20. C. Lesoil, T. Nonaka, H. Sekiguchi, T. Osada, M. Miyata, R. Afrin and A. Ikai, *Biochemical and Biophysical Research Communications*, 2010, **391**, 1312-1317.
21. L. Ge, G. Jin and X. Fang, *Langmuir*, 2012, **28**, 707-713.
22. B. F. Haynes, P. B. Gilbert, M. J. McElrath, S. Zolla-Pazner, G. D. Tomaras, S. M. Alam, D. T. Evans, D. C. Montefiori, C. Karnasuta, R. Sutthent, H.-X. Liao, A. L. DeVico, G. K. Lewis, C. Williams, A. Pinter, Y. Fong, H. Janes, A. DeCamp, Y. Huang, M. Rao, E. Billings, N. Karasavvas, M. L. Robb, V. Ngauy, M. S. de Souza, R. Paris, G. Ferrari, R. T. Bailer, K. A. Soderberg, C. Andrews, P. W. Berman, N. Frahm, S. C. De Rosa, M. D. Alpert, N. L. Yates, X. Shen, R. A. Koup, P. Pitisuttithum, J. Kaewkungwal, S. Nitayaphan, S. Rerks-Ngarm, N. L. Michael and J. H. Kim, *New England Journal of Medicine*, 2012, **366**, 1275-1286.
23. A. Ambrosi, F. Airò and A. Merkoçi, *Analytical Chemistry*, 2009, **82**, 1151-1156.
24. X. Wang, X. Lou, Y. Wang, Q. Guo, Z. Fang, X. Zhong, H. Mao, Q. Jin, L. Wu, H. Zhao and J. Zhao, *Biosensors and Bioelectronics*, 2010, **25**, 1934-1940.
25. P. Qian, S. Ai, H. Yin and J. Li, *Microchim Acta*, 2010, **168**, 347-354.
26. T. P. Brennan, P. Ardalan, H.-B.-R. Lee, J. R. Bakke, I. K. Ding, M. D. McGehee and S. F. Bent, *Advanced Energy Materials*, 2011, **1**, 1169-1175.
27. D. Samanta and A. Sarkar, *Chemical Society Reviews*, 2011, **40**, 2567-2592.
28. A. J. Read, D. S. Finlaison, X. Gu, R. J. Davis, K. E. Arzey and P. D. Kirkland, *Australian Veterinary Journal*, 2011, **89**, 42-43.
29. J. J. Luime, E. M. Colin, J. M. Hazes and E. Lubberts, *Annals of the rheumatic diseases*, 2010, **69**, 337-344.
30. C. A. Wagner, J. Sokolove, L. J. Lahey, C. Bengtsson, S. Saevarsdottir, L. Alfredsson, M. Delanoy, T. M. Lindstrom, R. P. Walker, R. Bromberg, P. E. Chandra, S. R. Binder, L. Klareskog and W. H. Robinson, *Annals of the rheumatic diseases*, 2015, **74**, 579-586.

31. Z. Szekanecz, L. Soos, Z. Szabo, A. Fekete, A. Kapitany, A. Vegvari, S. Sipka, G. Szucs, S. Szanto and G. Lakos, *Clinical reviews in allergy & immunology*, 2008, **34**, 26-31.
32. S. D. Gan and K. R. Patel, *J Invest Dermatol*, 2013, **133**, e12.
33. C. E. Soteropulos, H. K. Hunt and A. M. Armani, *Applied Physics Letters*, 2011, **99**, -.
34. P. Hinterdorfer and Y. F. Dufrene, *Nat Meth*, 2006, **3**, 347-355.
35. S. Freitag, I. Le Trong, L. Klumb, P. S. Stayton and R. E. Stenkamp, *Protein Science : A Publication of the Protein Society*, 1997, **6**, 1157-1166.
36. M. González, L. A. Bagatolli, I. Echabe, J. L. R. Arrondo, C. E. Argaraña, C. R. Cantor and G. D. Fidelio, *Journal of Biological Chemistry*, 1997, **272**, 11288-11294.
37. F. Rico and V. T. Moy, *Journal of Molecular Recognition*, 2007, **20**, 495-501.
38. J. A. Howarter and J. P. Youngblood, *Langmuir*, 2006, **22**, 11142-11147.
39. A. S. Campbell, C. Dong, J. S. Dordick and C. Z. Dinu, *Process Biochemistry*, 2013, **48**, 1355-1360.
40. J. P. Cleveland, S. Manne, D. Bocek and P. K. Hansma, *Review of Scientific Instruments*, 1993, **64**, 403-405.
41. B. Ohler, *Review of Scientific Instruments*, 2007, **78**, -.
42. O. K. Dudko, G. Hummer and A. Szabo, *Physical Review Letters*, 2006, **96**, 108101.
43. C. Yuan, A. Chen, P. Kolb and V. T. Moy, *Biochemistry*, 2000, **39**, 10219-10223.
44. J. Morfill, K. Blank, C. Zahnd, B. Luginbühl, F. Kühner, K.-E. Gottschalk, A. Plückthun and H. E. Gaub, *Biophysical journal*, 2007, **93**, 3583-3590.
45. S. S. Wong, E. Joselevich, A. T. Woolley, C. L. Cheung and C. M. Lieber, *Nature*, 1998, **394**, 52-55.
46. J. M. Teulon, Y. Delcuze, M. Odorico, S. W. Chen, P. Parot and J. L. Pellequer, *Journal of molecular recognition : JMR*, 2011, **24**, 490-502.
47. A. N. Leistra, J. H. Han, S. Tang, B. G. Orr, M. M. Banaszak Holl, S. K. Choi and K. Sinniah, *The Journal of Physical Chemistry B*, 2015, **119**, 5785-5792.
48. A. S. Campbell, C. Dong, F. Meng, J. Hardinger, G. Perhinschi, N. Wu and C. Z. Dinu, *ACS Applied Materials & Interfaces*, 2014, **6**, 5393-5403.
49. H. Schönherr, M. W. J. Beulen, J. Bügler, J. Huskens, F. C. J. M. van Veggel, D. N. Reinhoudt and G. J. Vancso, *Journal of the American Chemical Society*, 2000, **122**, 4963-4967.
50. S. Zou, H. Schönherr and G. J. Vancso, *Journal of the American Chemical Society*, 2005, **127**, 11230-11231.
51. C.-K. Lee, Y.-M. Wang, L.-S. Huang and S. Lin, *Micron*, 2007, **38**, 446-461.
52. G. Bell, *Science*, 1978, **200**, 618-627.
53. E. Evans and K. Ritchie, *Biophysical journal*, 1997, **72**, 1541-1555.
54. H. A. Kramers, *Physica*, 1940, **7**, 284-304.
55. A. R. Bizzarri and S. Cannistraro, *Chemical Society Reviews*, 2010, **39**, 734-749.
56. M. de Odrowaz Piramowicz, P. Czuba, M. Targosz, K. Burda and M. Szymonski, *Acta biochimica Polonica*, 2006, **53**, 93-100.
57. E. Galligan, C. J. Roberts, M. C. Davies, S. J. B. Tendler and P. M. Williams, *The Journal of Chemical Physics*, 2001, **114**, 3208-3214.
58. V. T. Moy, E.-L. Florin and H. E. Gaub, *Colloids and Surfaces A: Physicochemical and Engineering Aspects*, 1994, **93**, 343-348.
59. X. Han, R. Lee, T. Chen, J. Luo, Y. Lu and K.-W. Huang, *Sci. Rep.*, 2013, **3**.
60. M. Mozurkewich, J. J. Lamb and S. W. Benson, *The Journal of Physical Chemistry*, 1984, **88**, 6435-6441.
61. I. Lee and R. E. Marchant, *Surface Science*, 2001, **491**, 433-443.
62. I. Lee and R. E. Marchant, *Ultramicroscopy*, 2003, **97**, 341-352.
63. M. E. Craig, D. M. Crothers and P. Doty, *Journal of Molecular Biology*, 1971, **62**, 383-401.
64. S. Guo, N. Lad, C. Ray and B. B. Akhremitchev, *Biophysical journal*, 2009, **96**, 3412-3422.
65. M. E. Wiseman and C. W. Frank, *Langmuir*, 2012, **28**, 1765-1774.
66. M. G. Kim, J. H. Yang, K. M. Kim, C. H. Jang, J. Y. Jung, I. J. Cho, S. M. Shin and S. H. Ki, *Toxicological sciences : an official journal of the Society of Toxicology*, 2015.

Tables and Figures

Table 1: Bell Model Parameters from F vs ln(L_r) relationship

Ligand-protein complex	Loading rate (pN/s)	Energy barrier width $x^{\neq}$ (nm)	Dissociation rate constant in the absence of an external force k_0 (s^{-1})	Activation energy E (k_BT)
Anti-streptavidin antibody-streptavidin	11500 to 161000	1.73	10.19	-2.32
	18400 to 690000	0.097	2814	-7.94
Biotin-streptavidin	250 to 2500	0.84	3.64×10-9	19.44
	7500 to 150000	0.031	24.94	-3.2

Figure 1.

Concept drawing of surface functionalization and contact mode analysis performed using Atomic Force Microscopy (AFM). (a) Functionalization of streptavidin protein to the glass surfaces; functionalization was performed using covalent binding. (b) Functionalization of anti-streptavidin antibody or biotin to the AFM tip. Schematic representation of the rupture force between streptavidin and its ligands, i.e., anti-streptavidin antibodies (c), or biotin used as control (d) respectively.

Figure 2.

Binding forces between streptavidin and its ligands, namely anti-streptavidin antibodies and biotin used as control. (a) Contact mode force map analysis of the rupture force between representative anti-streptavidin antibody-coated tip and streptavidin-coated glass surface. (b) Contact mode force map analysis of the rupture force between representative biotin-coated tip and streptavidin-coated glass surface. The colored squares are associated with different values of the rupture forces being measured, with the darker representing smaller and brighter colors representing larger rupture forces respectively. (c) Representative distribution of the rupture forces between streptavidin-coated glass surface and anti-streptavidin antibody-coated tip. (d) Representative distribution of the rupture forces between streptavidin-coated glass surface and the biotin-coated tip. The distributions were obtained from independent force maps, with the two force maps for the individual ligands being analyzed being also representatives of all parallel experiments (n=12).

Figure 3.

Loading rate dependence on the rupture force in the unbinding process of the (a) anti-streptavidin antibody-streptavidin; and (b) biotin-streptavidin respectively. The x axis is the logarithm of the loading rate while the y axis represents the rupture force; 12 independent force maps were obtained for each of the protein-ligand being investigated.

Figure 4.

Histogram of the average rupture force between streptavidin and its ligands, with at least 240 independent force maps analyses being performed for each of the complexes being investigated. Control I and control II represents the average rupture force between biotin- and anti-streptavidin antibody-coated tip and the glass respectively (with at least 60 independent force maps for each of the controls). A Student T-test was carried out with the significance level of $p^{*}<0.05$; (*) indicates significance between individual complexes and the control while (***) indicates significant from the different complexes.

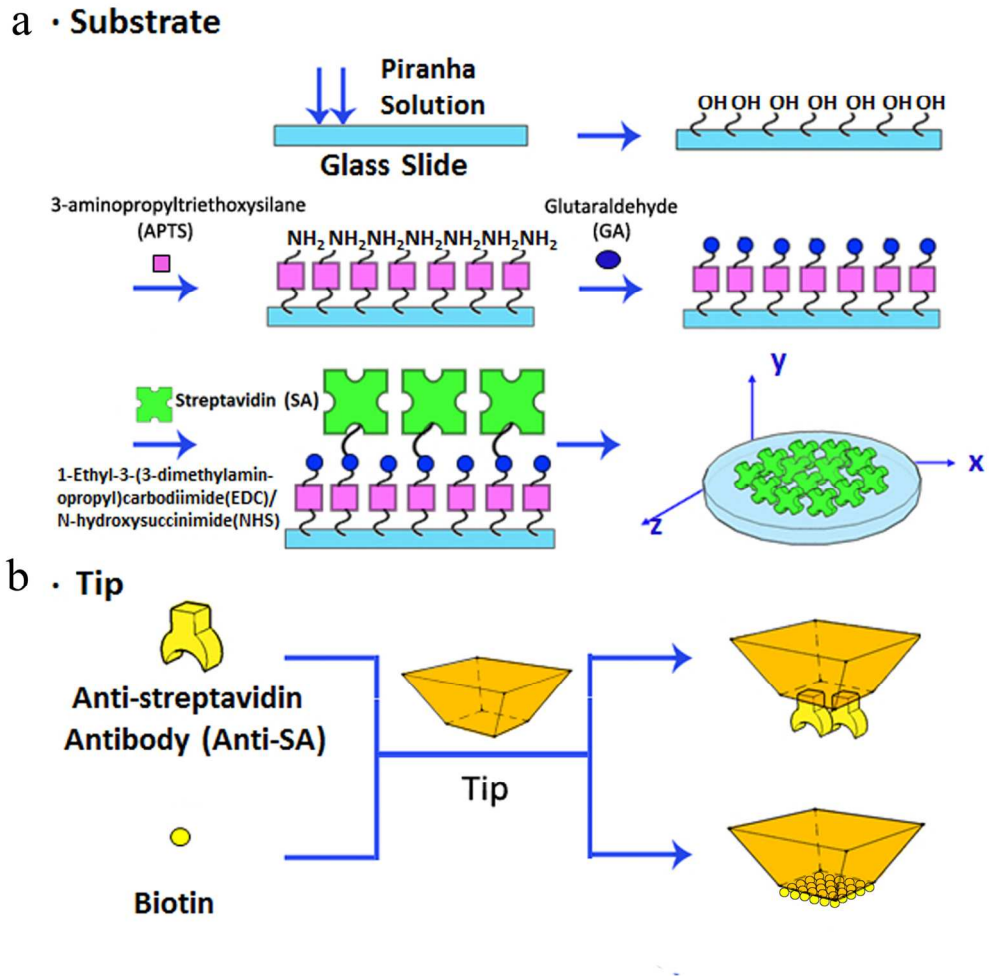

Figure 1: Concept drawing of surface functionalization and contact mode analysis performed using Atomic Force Microscopy (AFM). (a) Functionalization of streptavidin protein to the glass surfaces; functionalization was performed using covalent binding. (b) Functionalization of anti-streptavidin antibody or biotin to the AFM tip.
162x158mm (300 x 300 DPI)

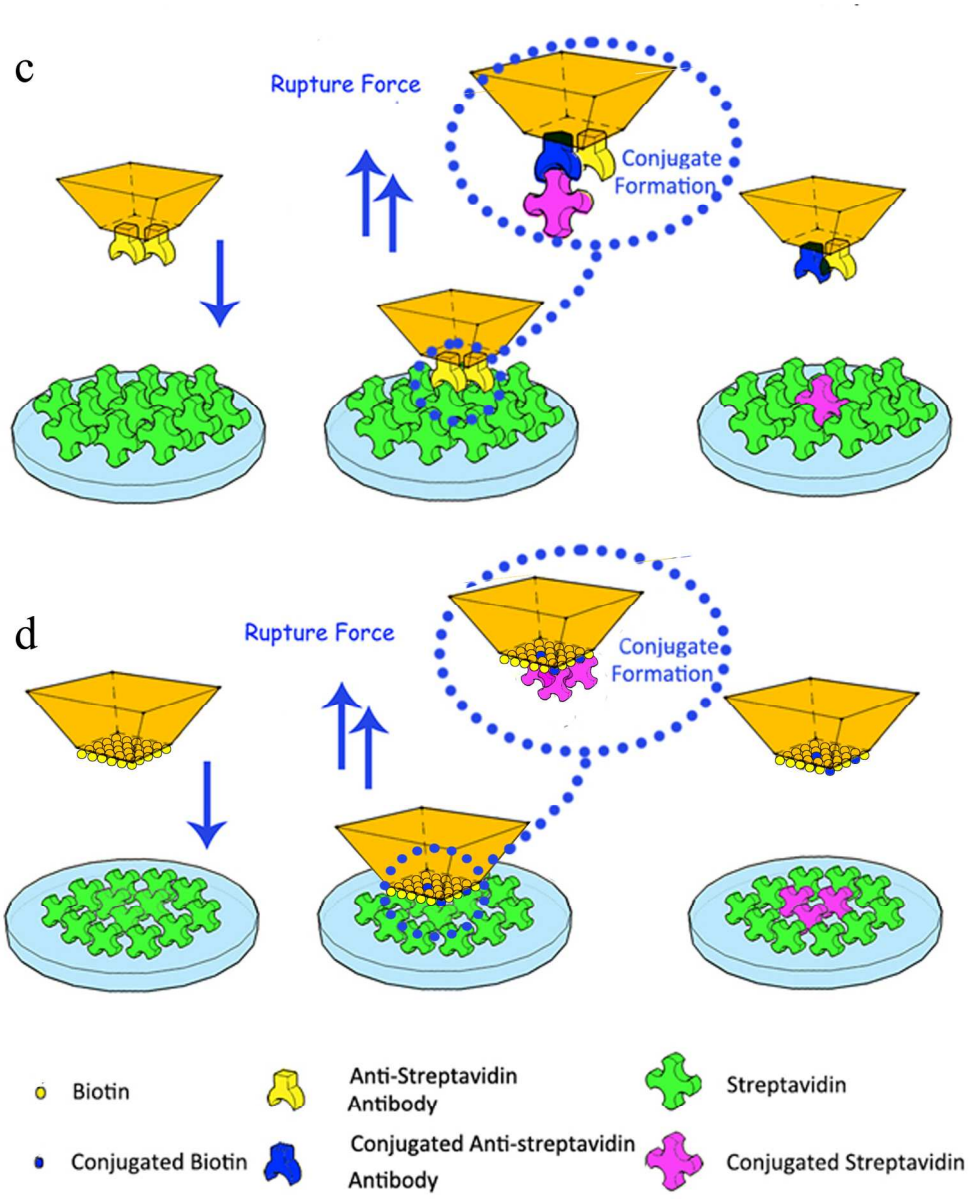

Figure 1: Schematic representation of the rupture force between streptavidin and its ligands, i.e., anti-streptavidin antibodies (c), or biotin used as control (d) respectively.
201x242mm (300 x 300 DPI)

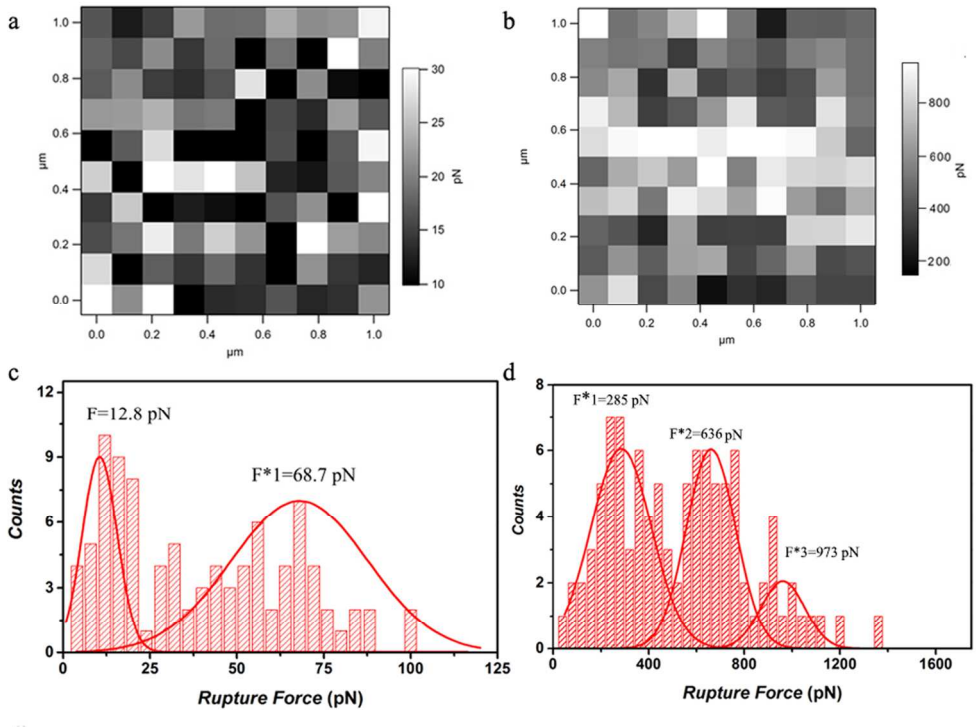

Figure 2: Binding forces between streptavidin and its ligands, namely anti-streptavidin antibodies and biotin used as control. (a) Contact mode force map analysis of the rupture force between representative anti-streptavidin antibody-coated tip and streptavidin-coated glass surface. (b) Contact mode force map analysis of the rupture force between representative biotin-coated tip and streptavidin-coated glass surface. The colored squares are associated with different values of the rupture forces being measured, with the darker representing smaller and brighter colors representing larger rupture forces respectively. (c) Representative distribution of the rupture forces between streptavidin-coated glass surface and anti-streptavidin antibody-coated tip. (d) Representative distribution of the rupture forces between streptavidin-coated glass surface and the biotin-coated tip. The distributions were obtained from independent force maps, with the two force maps for the individual ligands being analyzed being also representatives of all parallel experiments (n=12).
125x93mm (300 x 300 DPI)

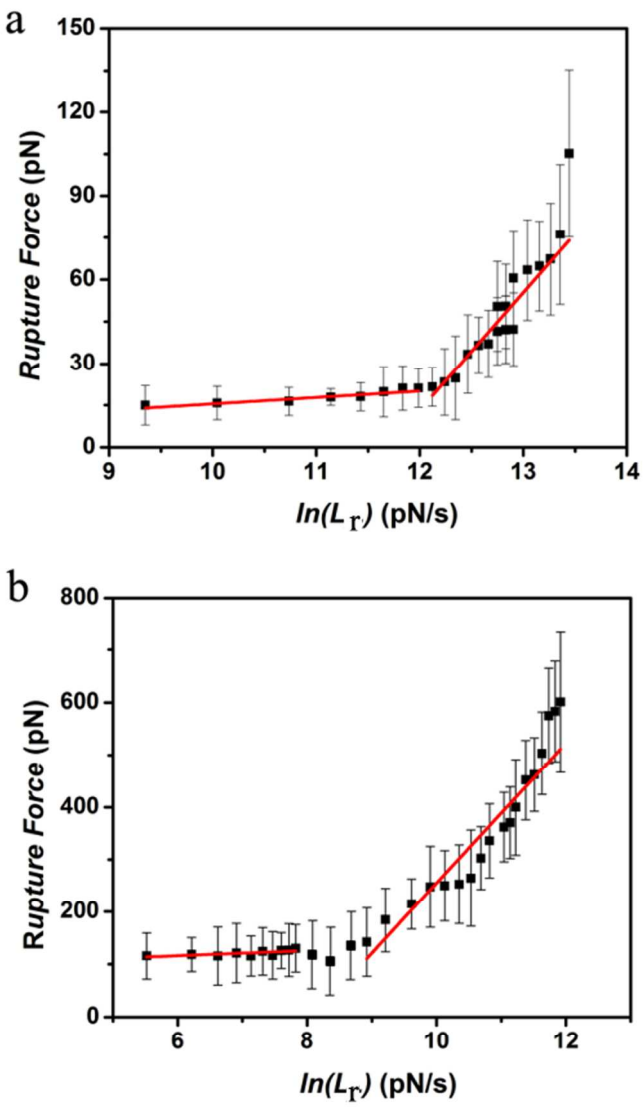

Figure 3: Loading rate dependence on the rupture force in the unbinding process of the (a) anti-streptavidin antibody-streptavidin; and (b) biotin-streptavidin respectively. The x axis is the logarithm of the loading rate while the y axis represents the rupture force; 12 independent force maps were obtained for each of the protein-ligand being investigated.
107x172mm (300 x 300 DPI)

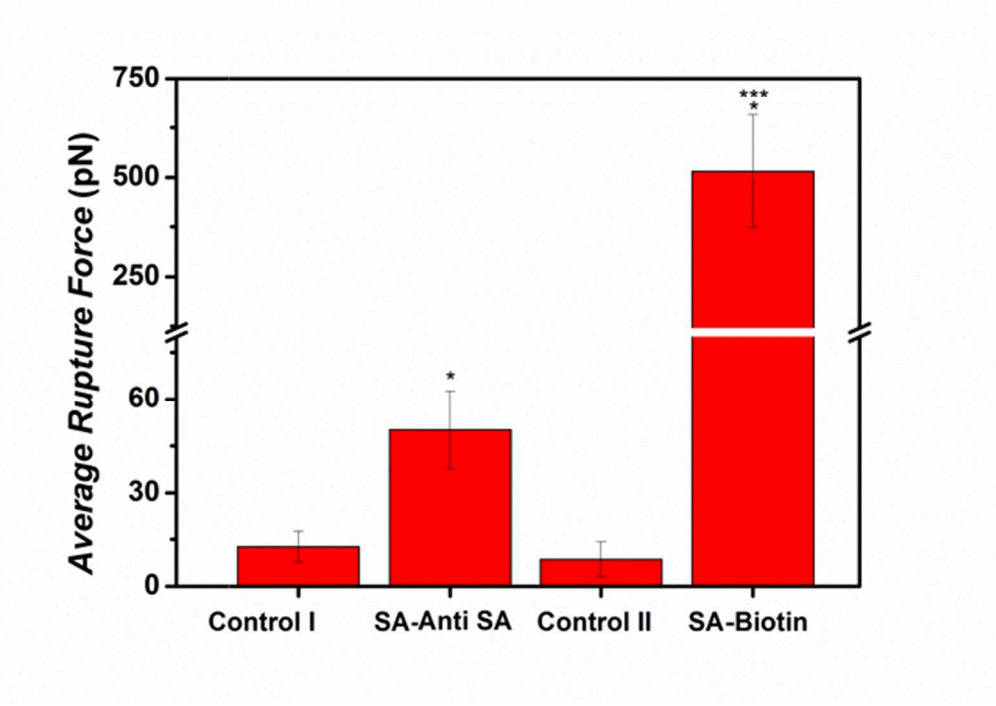

Figure 4: Histogram of the average rupture force between streptavidin and its ligands, with at least 240 independent force maps analyses being performed for each of the complexes being investigated. Control I and control II represents the average rupture force between biotin- and anti-streptavidin antibody-coated tip and the glass respectively (with at least 60 independent force maps for each of the controls). A Student T-test was carried out with the significance level of p*<0.05; (*) indicates significance between individual complexes and the control while (***) indicates significant from the different complexes.
170x120mm (300 x 300 DPI)